

Robust Tensor Recovery using Low-Rank Tensor Ring

Huyan Huang, Yipeng Liu, *Senior Member, IEEE*, Ce Zhu, *Fellow, IEEE*

Abstract—Robust tensor completion recovers the low-rank and sparse parts from its partially observed entries. In this paper, we propose the robust tensor ring completion (RTRC) model and rigorously analyze its exact recovery guarantee via TR-unfolding scheme, and the result is consistent with that of matrix case. We propose the algorithms for tensor ring robust principle component analysis (TRRPCA) and RTRC using the alternating direction method of multipliers (ADMM). The numerical experiment demonstrates that the proposed method outperforms the state-of-the-art ones in terms of recovery accuracy.

Index Terms—Tensor ring robust principle component analysis, Robust tensor ring completion, alternating direction method of multipliers

I. INTRODUCTION

IN practice, the acquired data are often slightly corrupted with small noises and hence present a rambling pattern, which results in a high-dimensional structure. As a widely used dimensionality reduction method, principle component analysis (PCA) extracts the most useful low-dimensional structure in observed data and reduces the unnecessary features. However, PCA suffers from the performance deterioration caused by grossly corruption. To address this issue, [1] considers the model as a superposition of low-rank matrix and the sparse noise and first gives the strong recovery guarantee for robust PCA (RPCA). Specifically, given an observed matrix \mathbf{T} and we wish to decompose it as $\mathbf{T} = \mathbf{L}_0 + \mathbf{S}_0$, where \mathbf{L} is a low-rank matrix and \mathbf{S} is a sparse matrix. Then the exact \mathbf{L}_0 and \mathbf{S}_0 is obtained by solving the convex program $\min_{\mathbf{L}, \mathbf{S}} \|\mathbf{L}\|_* + \lambda \|\mathbf{S}\|_1$, s. t. $\mathbf{L} + \mathbf{S} = \mathbf{T}$. The RPCA is applicable to a series of applications such as signal processing [2], machine learning [3], remote sensing [4], computer vision [5], etc.

A tensor is a multi-dimensional array that naturally represents the high-dimensional observation, and it is helpful for preserving more intrinsic structures and information than matrix when dealing with high-order data such as RGB images, light-field images and videos, etc [2], [6], [7]. It is ubiquitous that during data transmission parts of the data entries are not only missing but also (grossly) corrupted. RPCA is not able to perform well in this situation. Similar to RPCA, the most existing tensor methods are based on

the assumption of low-rank property [8]. However, the extension for RPCA of matrix to tensor is hard because of its algebraic problem [9]. There are two TRPCA methods. [10] first proposes an algorithm for tensor RPCA (TRPCA) that utilizes the sum of Tucker nuclear norm (SNN) and hence is called TRPCA-SNN. The Tucker nuclear norm is a suboptimal convex surrogate [11], [12] of Tucker-rank which is defined as $\text{rank}_{\text{Tucker}}(\mathcal{X}) = [\text{rank}(\mathbf{X}_{(1)}), \dots, \text{rank}(\mathbf{X}_{(d)})]$, where $\mathbf{X}_{(i)}$ is the tensor unfolding along its i -th dimension [6]. [13] provides the exact recovery guarantee for TRPCA-SNN. Tensor singular value decomposition (t-SVD) factorizes a 3-way tensor into two orthogonal tensors and a f-diagonal tensor based on the tensor-tensor product [14], and the tubal rank is defined as the number of non-vanishing tubes in the f-diagonal tensor [15]. [16] proves that the tensor nuclear norm (TNN) is the convex envelop of tubal rank and proposes a method called TRPCA-TNN for TRPCA with strong recovery guarantee. This is the second TRPCA approach. The corresponding model can be represented as $\min_{\mathcal{L}, \mathcal{S}} \|\mathcal{L}\|_* + \lambda \|\mathcal{S}\|_1$, s. t. $\mathcal{L} + \mathcal{S} = \mathcal{T}$.

The recently proposed tensor ring (TR) decomposition decomposes a high-order tensor as a sequence of cyclically contracted 3-order tensors [17], [18]. The cycle forces TR-rank to be small and TR-rank is consistently invariant under the cyclic permutation of the factors. [19], [20] show that the TR model has the advantage of powerful representation ability compared with other decompositions such as tensor train (TT) and Tucker. [21] proposes a balanced TR-unfolding scheme for tensor completion and shows performance improvement. [22] proposes an approach for tensor completion using TR nuclear norm minimization and provides the exact recovery guarantee. This method achieves better performance than the existing ones. Follow [22], we extend our analysis to TRPCA. Our contributions are itemized as follows:

- 1) We rigorously analyze the sampling condition for TR-PCA using the TR model, in which only one TR-unfolding suffices to yield the exact recovery. Inspired by this finding, we propose two algorithms that yield the exact recovery with high probability for robust PCA and robust completion using the TR decomposition. The two methods are called tensor ring robust PCA (TRRPCA) and robust TR completion (RTRC), respectively.
- 2) We use an alternating direction method of multipliers (ADMM) to solve two proposed models. The numerical experiments show the performance improvement in practical applications such as RGB image recovery and background modeling.

The organization for the remainder of this paper is ar-

This research is supported by National Natural Science Foundation of China (NSFC, No. 61602091, No. 61571102). The corresponding author is Yipeng Liu.

All the authors are with School of Information and Communication Engineering, University of Electronic Science and Technology of China (UESTC), Chengdu, 611731, China. (email: huyanhuang@gmail.com, yipengliu@uestc.edu.cn).

ranged as follows. In section II, the basic notations of TR decomposition are introduced. In section III, we develop the analysis for robust TR completion. In section IV, we introduce two algorithms for TRPCA and its robust version. Section V displays the experimental results. Finally we conclude our work in section VI.

II. NOTATIONS AND PRELIMINARIES

A. Notations about tensor ring decomposition

This section introduces some basic notations of tensors. A scalar, a vector, a matrix and a tensor are denoted by normal letter, boldface lowercase letter, boldface uppercase letter and calligraphic letter, respectively. For instance, a d -order tensor is denoted as $\mathcal{X} \in \mathbb{R}^{n_1 \times \dots \times n_d}$, where n_i is the size corresponding to dimension i , $i \in \{1, \dots, d\}$. An entry of the tensor \mathcal{X} is denoted as $x_{j_1 \dots j_d}$, where j_i is the index with mode i , $1 \leq j_i \leq n_i$. A mode- i fiber of \mathcal{X} can be denoted as $\mathbf{x}_{j_1 \dots j_{i-1} j_{i+1} \dots j_d}$, and $\mathbf{X}_{\dots j_i \dots}$ represents the slice along mode i .

$\|\mathbf{X}\|_2 = \sigma_{\max}(\mathbf{X})$ denotes the spectral norm of the matrix \mathbf{X} , which is equal to its maximal singular value. We regard \mathbf{E} as the identity matrix. The inner product of two tensors \mathcal{X} and \mathcal{Y} is defined as $\langle \mathcal{X}, \mathcal{Y} \rangle = \sum_{j_1=1}^{n_1} \dots \sum_{j_d=1}^{n_d} x_{j_1 \dots j_d} y_{j_1 \dots j_d}$. The Frobenius norm of a tensor \mathcal{X} can be defined as $\|\mathcal{X}\|_F = \sqrt{\langle \mathcal{X}, \mathcal{X} \rangle}$. The Kronecker product is written as $\mathbf{X} \otimes \mathbf{Y}$. The Hadamard product \otimes is an element-wise product which is $\mathbf{X} \otimes \mathbf{Y}$.

Mode- i unfolding maps a tensor to a matrix $\mathbf{X}_{(i)} \in \mathbb{R}^{n_i \times J_i}$ by rearranging the fibers as the columns of the matrix. i.e., $x_{j_1 \dots j_d} = x_{j_n j}$, and $j = \overline{j_1 \dots j_{i-1} j_{i+1} \dots j_d}$ is $j = 1 + \sum_{i=1, i \neq k}^d (j_i - 1) \prod_{m=1, m \neq k}^{i-1} n_m$. Mode- i matricization unfolds a tensor along its first i modes [19], i.e., $\mathbf{X}_{[i]} \in \mathbb{R}^{\prod_{k=1}^i n_k \times \prod_{k=i+1}^d n_k}$. In the context of TR decomposition, $\mathbf{X}_{\{i,l\}}$ denotes the i -shifting l -matricization of the tensor \mathcal{X} . It firstly permutes the tensor with order $[i, \dots, d, 1, \dots, i-1]$ and performs matricization along first l modes. As a special case of i -shifting l -matricization, i -shifting balanced unfolding $\mathbf{X}_{(i)} \in \mathbb{R}^{n_i \times \dots \times n_{i+\lfloor d/2 \rfloor} \times n_{i+\lfloor d/2 \rfloor+1} \times \dots \times n_d \times n_1 \times \dots \times n_{d-1}}$ permutes a tensor with order $[i, \dots, d, 1, \dots, i-1]^T$ and unfolds tensor along its first $\lfloor d/2 \rfloor$ modes. The indices of $(\mathbf{X}_{(k)})_{pq}$ can be formulated as $p = 1 + \sum_{i=k}^{k-1+d/2} (j_i - 1) \prod_{m=k}^{i-1} n_m$ and $q = 1 + \sum_{i=k+d/2}^{k-1} (j_i - 1) \prod_{m=k+d/2}^{i-1} n_m$.

Let $\{\mathcal{G}\} = \{\mathcal{G}^{(1)}, \dots, \mathcal{G}^{(d)}\}$ denote the cores of TR decomposition and the TR rank be $[r_1, \dots, r_N]^T$, where $\mathcal{G}^{(n)} \in \mathbb{R}^{r_k \times n_k \times r_{k+1}}$. Then the scalar form of TR decomposition can be written as $x_{j_1 \dots j_d} = \sum_{t_1=1}^{r_1} \dots \sum_{t_d=1}^{r_d} g_{t_1 j_1 t_2}^{(1)} \dots g_{t_{d-1} j_{d-1} t_d}^{(d-1)} g_{t_d j_d t_1}^{(d)}$. Equivalently, it can be represented by a more compact form $x_{j_1 \dots j_d} = \text{tr}(\mathbf{G}_{j_1}^{(1)} \dots \mathbf{G}_{j_d}^{(d)})$, where $\mathbf{G}_{j_k}^{(k)}$ is the j_k -th mode-2 slice of core $\mathcal{G}^{(k)}$, and $\text{tr}(\cdot)$ is the trace function. The tensorized representation is $\mathcal{X} = \sum_{t_1=1}^{r_1} \dots \sum_{t_d=1}^{r_d} \mathbf{g}_{t_1 t_2}^{(1)} \circ \dots \circ \mathbf{g}_{t_{d-1} t_d}^{(d-1)} \circ \mathbf{g}_{t_d t_1}^{(d)}$, where $\mathbf{g}_{t_k t_{k+1}}^{(k)}$ is the (t_k, t_{k+1}) -th mode-2 fiber of core $\mathcal{G}^{(k)}$, and \circ denotes the outer product.

We use \otimes to denote the tensor connection product. It combines several TR-cores into a new core and the formula

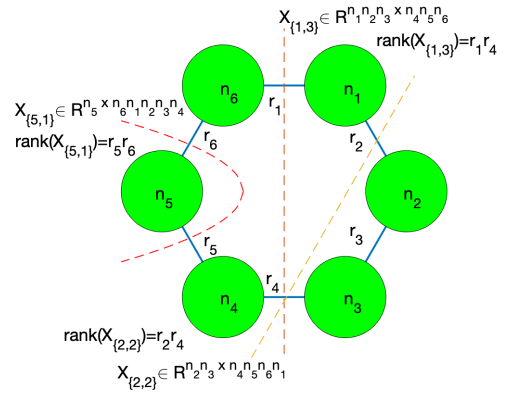


Fig. 1. An intuitive illustration of TR-rank and its unfolding's rank, in which the 6-order tensor is with the size of $n_1 \times \dots \times n_6$, and its TR rank is $[r_1, \dots, r_6]^T$. The dashed lines represent the unfolding processing.

is $\left(\overline{\otimes}_{n=a}^b \mathcal{G}^{(k)}\right)_{t_a: t_{b+1}} = \sum_{t_{a+1}=1}^{r_a} \dots \sum_{t_b=1}^{r_b} \mathbf{g}_{t_a t_{a+1}}^{(a)} \otimes \dots \otimes \mathbf{g}_{t_b t_{b+1}}^{(b)}$, where $\overline{\otimes}_{n=a}^b \mathcal{G}^{(k)} \in \mathbb{R}^{r_a \times (\prod_{i=a}^b n_i) \times r_{b+1}}$.

B. Preliminaries

This subsection reviews the existing TRPCA methods. Following the RPCA, [10], [13] first propose the approach called TRPCA-SNN which is based on the Tucker-rank and its convex relaxation:

$$\min_{\mathcal{X}} \sum_{i=1}^d w_i \|\mathbf{X}_{(i)}\|_* + \|\mathcal{S}\|_1, \text{ s. t. } \mathcal{P}_{\Omega}(\mathcal{X} + \mathcal{S}) = \mathcal{P}_{\Omega}(\mathcal{T}). \quad (1)$$

Then [16] proposes the TRPCA-TNN based on the tensor nuclear norm.

$$\min_{\mathcal{X}} \|\mathcal{X}\|_* + \|\mathcal{S}\|_1, \text{ s. t. } \mathcal{P}_{\Omega}(\mathcal{X} + \mathcal{S}) = \mathcal{P}_{\Omega}(\mathcal{T}). \quad (2)$$

III. SAMPLING FOR LOW-RANK TENSOR COMPLETION VIA TENSOR RING

This section introduces the main result of exact recovery guarantee for RTRC. [22] rigorously proves the relationship between TR-rank and TR-unfolding's rank, which is characterized in Fig. 1. Specifically, the rank of TR-unfolding $\mathbf{X}_{\{i,l\}}$ is $\text{rank}(\mathbf{X}_{\{i,l\}}) = r_i r_{i+l}$, $i \in \{1, \dots, d\}$, $l \in \{1, \dots, d-1\}$, provided that the TR-rank is $[r_1, \dots, r_d]^T$. Their study also indicates that it suffices to consider a (sub)critical TR for the TRPCA, and in the next a TR is short for a (sub)critical TR wherever it appears.

Since [22] implies the equivalence between TR decomposition and SVD decomposition, we are interested in finding the condition for exact recovery guarantee using one TR-unfolding. The following theorem characterizes our result.

Theorem 1 (Robust TR completion, uniformly bounded model). *Let a d -order tensor $\mathcal{X} \in \mathbb{R}^{n_1 \times \dots \times n_d}$ be sampled from a uniformly bounded model with TR-rank being $[r_1, \dots, r_d]$. Define \bar{n}_{kl} and \underline{n}_{kl} as the maximum and minimum values of $\left\{ \prod_{i=k}^{k+l-1} n_i, \prod_{i=k+l}^{k-1} n_i \right\}$. Then solving (5) with*

$\lambda_k = 1/\sqrt{p\bar{n}_{kl}}$ yields the exact and unique solution \mathcal{X} with probability at least $1 - C\bar{n}_{kl}^{-3}$, provided that

$$r_k r_{k+l} \leq C_p p \bar{n}_{kl} \mu^{-1} (\lceil d/2 \rceil \ln \bar{n}_{kl})^{-2}, \quad \gamma \leq C_\gamma, \quad (3)$$

where C , C_p and C_γ are positive numerical constants, and p is probability of random sampling.

IV. ROBUST TENSOR RING COMPLETION METHOD

According to Theorem 1 and basic algebraic knowledge, a good strategy to improve the sampling bound is to set $l = \lceil d/2 \rceil$ within the $\{i, l\}$ unfolding scheme. Then we derive model (4)

$$\begin{aligned} \min_{\mathcal{X}^{(i)}, \mathcal{S}} \quad & \sum_{i=1}^{\lceil d/2 \rceil} w_i \|\mathcal{X}_{\langle i \rangle}^{(i)}\|_* + \lambda_i \|\mathcal{S}\|_1 \\ \text{s. t.} \quad & \mathcal{X}^{(i)} + \mathcal{S} = \mathcal{T}, \end{aligned} \quad (4)$$

in which the subscript $\{i, l\}$ is abbreviated to $\langle i \rangle$. This model is called tensor ring robust principle component analysis (TRRPCA).

Another model is an enhancement of model (4) since it incorporates the uniform and random sampling scheme. Consider the operator $\mathcal{A}_\Omega : \mathbb{R}^{n_1 \times \dots \times n_d} \mapsto \mathbb{R}^{m \times 1}$ as the sampling process where m is the number of samples, the corresponding model can be modified as

$$\begin{aligned} \min_{\mathcal{X}^{(i)}, \mathcal{L}, \mathcal{S}} \quad & \sum_{i=1}^{\lceil d/2 \rceil} w_i \|\mathcal{X}_{\langle i \rangle}^{(i)}\|_* + \lambda_i \|\mathcal{S}\|_1 \\ \text{s. t.} \quad & \mathcal{A}_\Omega(\mathcal{L} + \mathcal{S}) = \mathcal{A}_\Omega(\mathcal{T}) \\ & \mathcal{X}^{(i)} = \mathcal{L} \quad (i = 1, \dots, \lceil d/2 \rceil). \end{aligned} \quad (5)$$

We term this model as robust tensor ring completion (RTRC).

A. Algorithm for TRRPCA

In order to solve (4) using ADMM, we consider its augmented Lagrangian (AL) function

$$\begin{aligned} \min_{\mathcal{X}^{(i)}, \mathcal{S}} \quad & \lambda \|\mathcal{S}\|_1 + \sum_{i=1}^{\lceil d/2 \rceil} w_i \|\mathcal{X}_{\langle i \rangle}^{(i)}\|_* + \langle \mathcal{Z}^{(i)}, \mathcal{X}^{(i)} + \mathcal{S} - \mathcal{T} \rangle + \\ & \frac{\mu}{2} \|\mathcal{X}^{(i)} + \mathcal{S} - \mathcal{T}\|_{\mathbb{F}}^2. \end{aligned} \quad (6)$$

The solution to problem (6) is given as follows.

1) *Update of $\mathcal{X}^{(i)}$* : Taking the first-order derivative of objective function in (6) we have

$$\mathcal{O} \in \partial \frac{w_i}{\mu} \|\mathcal{X}_{\langle i \rangle}^{(i)}\|_* + \mathcal{X}^{(i)} - \left(\mathcal{T} - \mathcal{S} - \frac{1}{\mu} \mathcal{Z}^{(i)} \right),$$

which is the optimality condition of

$$\min_{\mathcal{X}^{(i)}} \frac{w_i}{\mu} \|\mathcal{X}_{\langle i \rangle}^{(i)}\|_* + \frac{1}{2} \|\mathcal{X}^{(i)} - \left(\mathcal{T} - \mathcal{S} - \frac{1}{\mu} \mathcal{Z}^{(i)} \right)\|_{\mathbb{F}}^2,$$

hence the optimal solution of $\mathcal{X}^{(i)}$ is

$$\mathcal{X}^{(i)*} = \text{D}_{\frac{w_i}{\mu}} \left(\mathcal{T} - \mathcal{S} - \frac{1}{\mu} \mathcal{Z}^{(i)} \right). \quad (7)$$

2) *Update of \mathcal{S}* : Follow the previous calculation there is

$$\mathcal{O} \in \partial \frac{\lambda}{\mu} \|\mathcal{S}\|_1 + \sum_{i=1}^{\lceil d/2 \rceil} \left[\mathcal{S} - \left(\mathcal{T} - \mathcal{X}^{(i)} - \frac{1}{\mu} \mathcal{Z}^{(i)} \right) \right]$$

which is the optimality condition of

$$\min_{\mathcal{S}} \frac{\lambda}{\mu} \|\mathcal{S}\|_1 + \sum_{i=1}^{\lceil d/2 \rceil} \frac{1}{2} \|\mathcal{S} - \left(\mathcal{T} - \mathcal{X}^{(i)} - \frac{1}{\mu} \mathcal{Z}^{(i)} \right)\|_{\mathbb{F}}^2.$$

By introducing the vector operator $\mathbf{1}$ the model becomes

$$\min_{\mathcal{S}} \frac{\lambda}{\mu} \|\mathcal{S}\|_1 + \frac{1}{2} \|\mathbf{1}\mathcal{S} - \left(\mathbf{1}\mathcal{T} - \vec{\mathcal{X}} - \frac{1}{\mu} \vec{\mathcal{Z}} \right)\|_{\mathbb{F}}^2,$$

the corresponding optimality condition is

$$\mathcal{O} \in \partial \frac{\lambda}{\mu} \|\mathcal{S}\|_1 + \mathbf{1}^T \mathbf{1}\mathcal{S} - \mathbf{1}^T \left(\mathbf{1}\mathcal{T} - \vec{\mathcal{X}} - \frac{1}{\mu} \vec{\mathcal{Z}} \right).$$

Rewrite the above representation as

$$\mathcal{O} \in \partial \frac{\lambda}{\lceil d/2 \rceil \mu} \|\mathcal{S}\|_1 + \mathcal{S} - \frac{1}{\lceil d/2 \rceil} \sum_{i=1}^{\lceil d/2 \rceil} \left(\mathcal{T} - \mathcal{X}^{(i)} - \frac{1}{\mu} \mathcal{Z}^{(i)} \right),$$

it is the solution to

$$\min_{\mathcal{S}} \frac{\lambda}{\lceil d/2 \rceil \mu} \|\mathcal{S}\|_1 + \frac{1}{2} \|\mathcal{S} - \frac{1}{\lceil d/2 \rceil} \sum_{i=1}^{\lceil d/2 \rceil} \left(\mathcal{T} - \mathcal{X}^{(i)} - \frac{1}{\mu} \mathcal{Z}^{(i)} \right)\|_{\mathbb{F}}^2,$$

thereby the update is

$$\mathcal{S}^* = \text{S}_{\frac{\lambda}{\lceil d/2 \rceil \mu}} \left(\frac{1}{\lceil d/2 \rceil} \sum_{i=1}^{\lceil d/2 \rceil} \left(\mathcal{T} - \mathcal{X}^{(i)} - \frac{1}{\mu} \mathcal{Z}^{(i)} \right) \right). \quad (8)$$

3) *Update of $\mathcal{Z}^{(i)}$* : Consider the scheme of dual ascent, the update of $\mathcal{Z}^{(i)}$ is given by

$$\mathcal{Z}^{(i)} = \mathcal{Z}^{(i)} + \mu \left(\mathcal{X}^{(i)} + \mathcal{S} - \mathcal{T} \right). \quad (9)$$

The pseudocode of TR robust PCA (TRRPCA) is outlined in Algorithm 1. A simplified version is taking one balanced unfolding within the model (4),

Algorithm 1 Tensor Ring Robust PCA (TRRPCA)

Input: Full observed tensor \mathcal{T} , penalty coefficient μ , number of maximal iterations K .

Output: Recovered low-rank tensor \mathcal{L} and sparse tensor \mathcal{S} .

- 1: Initialization $\mathcal{L}_0 = \mathcal{T}$, $\mathcal{S}_0 = \mathcal{O}$, $\{\mathcal{X}\} = \mathcal{L}_0$, $\{\mathcal{Z}\} = \mathcal{O}$.
 - 2: **for** $k = 1$ **to** K **do**
 - 3: **for** $i = 1$ **to** $\lceil d/2 \rceil$ **do**
 - 4: Update $\mathcal{X}^{(i)}$ according to (7)
 - 5: **end for**
 - 6: Update \mathcal{S} according to (8)
 - 7: **for** $i = 1$ **to** $\lceil d/2 \rceil$ **do**
 - 8: Update $\mathcal{Z}^{(i)}$ according to (9)
 - 9: **end for**
 - 10: **end for**
 - 11: $\mathcal{L} = \frac{1}{\lceil d/2 \rceil} \sum_{i=1}^{\lceil d/2 \rceil} \mathcal{X}^{(i)}$
 - 12: **return** \mathcal{L} and \mathcal{S}
-

B. Algorithm for RTRC

The AL function of model (5) is

$$\min_{\mathcal{X}^{(i)}, \mathcal{L}, \mathcal{S}} \lambda \|\mathcal{S}\|_1 + \sum_{i=1}^{\lceil d/2 \rceil} w_i \|\mathcal{X}^{(i)}\|_* + \langle \mathcal{Z}^{(i)}, \mathcal{X}^{(i)} - \mathcal{L} \rangle + \frac{\mu}{2} \|\mathcal{X}^{(i)} - \mathcal{L}\|_{\mathbb{F}}^2 + \langle \mathbf{w}, \mathcal{A}_{\Omega}(\mathcal{L} + \mathcal{S} - \mathcal{T}) \rangle + \frac{\mu}{2} \|\mathcal{A}_{\Omega}(\mathcal{L} + \mathcal{S}) - \mathcal{A}_{\Omega}(\mathcal{T})\|_2^2. \quad (10)$$

1) *Update of $\mathcal{X}^{(i)}$* : Similar to the solution given in (7), the optimality condition

$$\mathcal{O} \in \partial \frac{w_i}{\mu} \|\mathcal{X}^{(i)}\|_* + \mathcal{X}^{(i)} - \left(\mathcal{L} - \frac{1}{\mu} \mathcal{Z}^{(i)} \right)$$

of (5) is also that of

$$\min_{\mathcal{X}^{(i)}} \frac{w_i}{\mu} \|\mathcal{X}^{(i)}\|_* + \frac{1}{2} \|\mathcal{X}^{(i)} - \left(\mathcal{L} - \frac{1}{\mu} \mathcal{Z}^{(i)} \right)\|_{\mathbb{F}}^2,$$

and the solution is

$$\mathcal{X}^{(i)*} = \mathbb{D}_{\frac{w_i}{\mu}} \left(\mathcal{L} - \frac{1}{\mu} \mathcal{Z}^{(i)} \right), \quad (11)$$

2) *Update of \mathcal{L}* : Denote by \mathcal{A}_{Ω}^* the adjoint of \mathcal{A}_{Ω} , the optimality condition is

$$\mathcal{O} \in \sum_{i=1}^{\lceil d/2 \rceil} -\mathcal{Z}^{(i)} + \mathcal{A}_{\Omega}^*(\mathbf{w}) + \sum_{i=1}^{\lceil d/2 \rceil} \mu \left(\mathcal{L} - \mathcal{X}^{(i)} \right) + \mu \mathcal{A}_{\Omega}^* \mathcal{A}_{\Omega}(\mathcal{L} + \mathcal{S} - \mathcal{T}).$$

Note that $\mathcal{A}_{\Omega}^*(\mathbf{w}) = \mathcal{P}_{\Omega}(\mathcal{W})$ and $\mathcal{A}_{\Omega}^* \mathcal{A}_{\Omega} = \mathcal{P}_{\Omega}$, we have

$$\mathcal{O} \in \sum_{i=1}^{\lceil d/2 \rceil} -\mathcal{Z}^{(i)} + \mathcal{P}_{\Omega}(\mathcal{W}) + \sum_{i=1}^{\lceil d/2 \rceil} \mu \left(\mathcal{L} - \mathcal{X}^{(i)} \right) + \mu \mathcal{P}_{\Omega}(\mathcal{L} + \mathcal{S} - \mathcal{T}).$$

Reformulate the formula as

$$\left(\lceil d/2 \rceil \mathcal{E} + \mathcal{P}_{\Omega} \right) (\mathcal{L}) = \sum_{i=1}^{\lceil d/2 \rceil} \left[\mathcal{X}^{(i)} + \frac{1}{\mu} \mathcal{Z}^{(i)} \right] + \mathcal{P}_{\Omega} \left(\mathcal{T} - \mathcal{S} - \frac{1}{\mu} \mathcal{W} \right),$$

and this leads to the rule of update

$$\mathcal{L}^* = \left\{ \sum_{i=1}^{\lceil d/2 \rceil} \left[\mathcal{X}^{(i)} + \frac{1}{\mu} \mathcal{Z}^{(i)} \right] + \mathcal{P} \circledast \left(\mathcal{T} - \mathcal{S} - \frac{1}{\mu} \mathcal{W} \right) \right\} \circledast \left(\lceil d/2 \rceil \mathcal{I} + \mathcal{P} \right), \quad (12)$$

where \mathcal{E} is the identity operator, \mathcal{I} is a tensor that fills with ones and \circledast represents the element-wise division.

3) *Update of \mathcal{S}* : Similar to the update of \mathcal{L} , the optimality condition is

$$\mathcal{O} \in \partial \frac{\lambda}{\mu} \|\mathcal{S}\|_1 + \mathcal{P}_{\Omega}(\mathcal{S}) - \mathcal{P}_{\Omega} \left(\mathcal{T} - \mathcal{L} - \frac{1}{\mu} \mathcal{W} \right),$$

which induces the equivalent model

$$\min_{\mathcal{S}} \frac{1}{2} \|\mathcal{A}_{\Omega}(\mathcal{S}) - \mathcal{A}_{\Omega} \left(\mathcal{T} - \mathcal{L} - \frac{1}{\mu} \mathcal{W} \right)\|_{\mathbb{F}}^2 + \frac{\lambda}{\mu} \|\mathcal{S}\|_1.$$

According to Lemma 1, the optimal solution is

$$\mathcal{S}^* = \mathbb{S}_{\frac{\lambda}{\mu}} \left(\mathcal{P} \circledast \left(\mathcal{T} - \mathcal{L} - \frac{1}{\mu} \mathcal{W} \right) \right). \quad (13)$$

Lemma 1. *The solution to optimization*

$$\min_{\mathcal{X}} \frac{1}{2} \|\mathcal{A}_{\Omega}(\mathcal{X}) - \mathcal{A}_{\Omega}(\mathcal{B})\|_2^2 + \tau \|\mathcal{X}\|_1$$

is $\mathcal{X}^* = \mathbb{S}_{\tau}(\mathcal{P} \circledast \mathcal{B})$, where \mathcal{P} is the binary sampling tensor.

4) *Update of $\mathcal{Z}^{(i)}$* : It is easy to calculate the update of dual variable $\mathcal{Z}^{(i)}$

$$\mathcal{Z}^{(i)} = \mathcal{Z}^{(i)} + \mu \left(\mathcal{X}^{(i)} - \mathcal{L} \right). \quad (14)$$

5) *Update of \mathcal{W}* : According to the rule of ADMM, the vector form of update is

$$\mathbf{w} = \mathbf{w} + \mu \mathcal{A}_{\Omega}(\mathcal{L} + \mathcal{S} - \mathcal{T}),$$

rewrite the formulation in a tensor form we derive

$$\mathcal{W} = \mathcal{W} + \mu \mathcal{P} \circledast (\mathcal{L} + \mathcal{S} - \mathcal{T}). \quad (15)$$

Algorithm 2 Robust Tensor Ring Completion (RTRC)

Input: Zero-filled observed tensor \mathcal{T} , observation set Ω , penalty coefficient μ , number of maximal iterations K .

Output: Recovered low-rank tensor \mathcal{L} and sparse tensor \mathcal{S} .

- 1: Initialization $\mathcal{P}, \mathcal{L}_0 = \mathcal{P} \circledast \mathcal{T}, \mathcal{S}_0 = \mathcal{O}, \{\mathcal{X}\} = \mathcal{L}_0, \{\mathcal{Z}\} = \mathcal{W} = \mathcal{O}$.
 - 2: **for** $k = 1$ **to** K **do**
 - 3: **for** $i = 1$ **to** $\lceil d/2 \rceil$ **do**
 - 4: Update $\mathcal{X}^{(i)}$ according to (11)
 - 5: **end for**
 - 6: Update \mathcal{L} according to (12)
 - 7: Update \mathcal{S} according to (13)
 - 8: **for** $i = 1$ **to** $\lceil d/2 \rceil$ **do**
 - 9: Update $\mathcal{Z}^{(i)}$ according to (14)
 - 10: **end for**
 - 11: Update \mathcal{W} according to (15)
 - 12: **end for**
 - 13: **return** \mathcal{L} and \mathcal{S}
-

C. Algorithmic complexity

We adopt the Lanczos algorithm introduced in [23] and [24] for the fast computation of SVD, since it has a linear complexity $O(p+q)$ for a p -by- q matrix. For a d -order hypercubic tensor $\mathcal{X} \in \mathbb{R}^{n \times \dots \times n}$ with TR-rank being $[r, \dots, r]$, the complexities of TRRPCA and RTRC algorithms mainly depend on the updates of \mathcal{X} which involve $d/2$ soft thresholdings and hence cost $O(dn^{d/2})$. The storage complexities of two algorithms are both $dn^{d/2}r^2$, since $d/2$ outcomes of SVDs are stored.

D. Algorithmic convergence

The ADMM algorithm has a linear rate of convergence when one of the objective terms is strongly convex [25]. Reference [26] provides a rather simple but efficient strategy to improve convergence, in which the penalty coefficient μ increases geometrically with iterations, i.e., $\mu_{k+1} = \beta\mu_k$, where β is a numerical constant.

V. NUMERICAL EXPERIMENTS

In this section, three groups of datasets are used for tensor completion experiments, i.e., synthetic data, real-world images and videos. Two algorithms are used to test the performance on real-world data, consisting of tensor robust PCA via tensor nuclear norm minimization (TRPCA-TNN) [27] and the proposed one. All the experiments are conducted in MATLAB 9.3.0 on a computer with a 2.8GHz CPU of Intel Core i7 and a 16GB RAM.

There are several evaluations for the quality of visual data. Relative error (RE), short for the root of relative squared error, is a common indicator for recovery accuracy, which is defined as

$$RE = \|\hat{\mathcal{X}} - \mathcal{X}\|_{\mathbb{F}} / \|\mathcal{X}\|_{\mathbb{F}}, \quad (16)$$

where \mathcal{X} is the ground truth and $\hat{\mathcal{X}}$ is the recovered tensor.

The second quality metric is peak signal-to-noise ratio, often abbreviated PSNR, is the ratio between the maximum possible power of a signal and the power of corrupting noise [28]. Given the ground truth \mathcal{X} and the estimation $\hat{\mathcal{X}}$, the mean squared error (MSE) is defined as

$$MSE = \frac{\|\hat{\mathcal{X}} - \mathcal{X}\|_{\mathbb{F}}^2}{\text{card}(\mathcal{X})}, \quad (17)$$

then the PSNR (in dB) is defined as

$$PSNR = 20 \lg \left(M / \sqrt{MSE} \right), \quad (18)$$

where M is the maximal pixel value which is 255 for the RGB images and videos, and $\text{card}(\cdot)$ represents the number of elements in a set. A higher PSNR usually indicates a higher quality of the reconstruction.

The third assessment is called structural similarity index (SSIM) which is used for measuring the similarity between the recovered image and original image [29]. It is calculated on various windows of an image. The measure between two windows X and Y of common size $N \times N$ is

$$SSIM_{XY} = \frac{(2\mu_X\mu_Y + c_1)(2\sigma_{XY} + c_2)}{(\mu_X^2 + \mu_Y^2 + c_1)(\sigma_X^2 + \sigma_Y^2 + c_2)}, \quad (19)$$

where μ_X and μ_Y are the averages of X and Y , σ_X and σ_Y are the variances of X and Y , $c_1 = (k_1L)^2$ and $c_2 = (k_2L)^2$ are two variables to stabilize the denominator (default values for k_1 and k_2 are 0.01 and 0.03), $L = 2^{\#\text{bits per pixel}} - 1$ is the dynamic range of pixel-values.

The last one quantifying the algorithmic complexity is the computational CPU time (in seconds).

The sampling ratio (SR) is defined as the ratio of the number of sampled entries to the number of the elements in tensor \mathcal{X} , noted as $SR = \text{card}(\odot) / \text{card}(\mathcal{X})$.

For fair comparisons, the parameters in each algorithm are tuned to give optimal performance, and all trials are repeated adequate times for avoiding fortuitous results. In our algorithm, μ_0 is set to be 1×10^{-3} . The convergence is determined by the relative change (RC) $RC = \|\mathcal{X}_k - \mathcal{X}_{k-1}\|_{\mathbb{F}} / \|\mathcal{X}_{k-1}\|_{\mathbb{F}}$, where the tolerance is set to be 1×10^{-5} . The number of maximal iterations is 100.

In the rest of this section, the experiments on real-world data including images and videos are used to test the performance of the proposed algorithms and others.

A. Images

Eight RGB images are tested in this section's experiment, including *airplane*, *baboon*, *barbara*, *facade*, *house*, *lena*, *peppers* and *sailboat*. The sizes of these images are all $256 \times 256 \times 3$. In image recovery, we randomly set 10% pixels with their values being randomly distributed from 0 to 255. The pixels are simultaneously chosen from red, green and blue channels, which is more difficult to recovery than the case of random sparse noise. The parameter settings are $\beta = 1.1$ and $\mu_0 = 1 \times 10^{-3.2}$. The visual data tensorization (VDT) method introduced in [19] and [30] can improve the performance, as a higher-order tensor makes it more efficient to exploit the local structures in original tensor and, if a tensor is slightly correlated, the tensorized one is more likely to have a low rank [19]. VDT first transforms an image into a real ket of a Hilbert space by casting the image to a higher-order tensor with an appropriate block structured addressing, i.e., tensorizing an image of size $M \times N \times 3$ to a tensor of size $m_1 \times \dots \times m_K \times n_1 \dots \times n_K \times 3$. Then VDT permutes and reshapes the resulting tensor into another one with size $m_1n_1 \times \dots \times m_Kn_K \times 3$. For these images, we use $[2 * \text{ones}(1, 16), 3]$ to reshape it and finally get a $[4 * \text{ones}(1, 8), 3]$ sized tensor. Note that the tensorizations are manually operated, and different operations will cause other results.

After applying the VDT manipulation, we compare the proposed method with the state-of-the-art algorithms. The recovery results including PSNR and CPU time of 2 algorithms, based on an average of 10 repetitions, are exhibited in Fig. V-A. The result shows the proposed methods prevail over other ones in terms of both PSNR and CPU time.

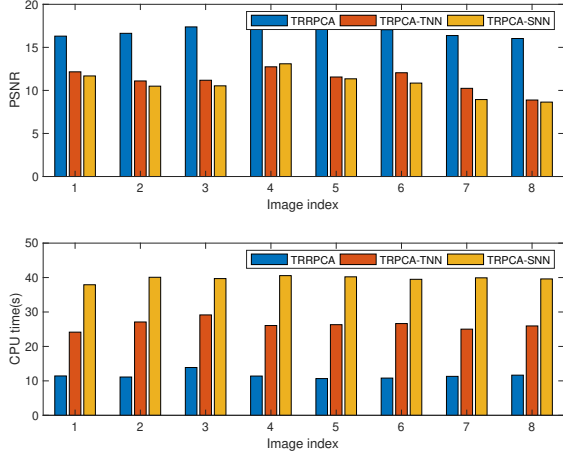
B. Real-world videos

In this group of experiments, a video are used to test the algorithms and each video recovery is repeated 5 times. The first is a color video called *pendulum* can be found in MATLAB with the size of $288 \times 352 \times 3 \times 50$. The video is further reshaped into a 9D tensor with the size of $4 \times 4 \times 4 \times 4 \times 4 \times 9 \times 11 \times 3 \times 2 \times 5 \times 5$ by VDT method. We set $\beta = 1.1$ and $\mu_0 = 1 \times 10^{-3}$.

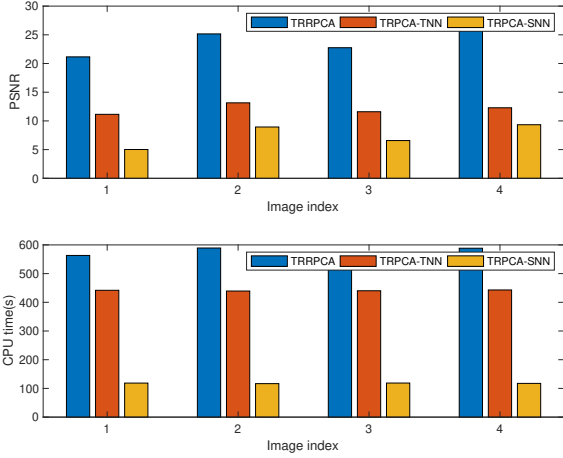
Fig. 2 gives the completion results of seven methods.

VI. CONCLUSION

Based on existing analysis of TR completion, we extend the analysis of exact recovery condition for robust tensor



(a) Comparison of the PSNR and CPU time derived form TRRPCA, TRPCA-TNN and TRPCA-SNN.



(b) Comparison of the PSNR and CPU time derived form TRRPCA, TRPCA-TNN and TRPCA-SNN.

ring completion. The result shows a similar lower bound to that of matrix case. Equipped with this foundation and based on a balanced TR-unfolding scheme, two algorithms named TRRPCA and RTRC are proposed to deal with the robust tensor completion, which show better performance against other state-of-the-art methods in application of visual data recovery and background modeling.

APPENDIX A PROOF OF THEOREM 1

Proof. The dual certificate for RTRC is that there is an unfolding $\mathbf{Y}_{\{k,l\}}$ such that the following conditions are satisfied:

$$\begin{cases} \left\| \frac{1}{(1-2\gamma)p} \mathcal{P}_{T_{kl}} \mathcal{P}_{\Psi_{kl}} \mathcal{P}_{T_{kl}} - \mathcal{P}_{T_{kl}} \right\|_2 < \frac{1}{2} & (20) \\ \left\| \mathcal{P}_{T_{kl}} (\mathbf{Y}_{\{k,l\}}) - \mathcal{P}_{T_{kl}} (\lambda_k \mathbf{N}_{\{k,l\}} - \mathbf{R}_{\{k,l\}}) \right\|_F \leq \prod_{i=1}^d n_i^{-1} \\ \left\| \mathcal{P}_{T_{kl}^\perp} (\mathbf{Y}_{\{k,l\}}) - \mathcal{P}_{T_{kl}^\perp} (\lambda_k \mathbf{N}_{\{k,l\}}) \right\|_2 \leq \frac{w_k}{2\lambda_k} \\ \mathcal{P}_{\Psi_{kl}^\perp} (\mathbf{Y}_{\{k,l\}}) = \mathbf{0} \\ \left\| \mathbf{Y}_{\{k,l\}} \right\|_\infty \leq \frac{1}{2} \end{cases}, \quad (21)$$

where $\mathcal{R} = \mathcal{R}(\{\mathcal{G}\}) \prod_{i=1}^d r_i^{-1} \sum_{i=1}^{\lfloor d/2 \rfloor} w_i r_i r_{i+1} \bar{n}_{il}$ and $\lambda_k = 1/\sqrt{p\bar{n}_{kl}}$. The operator $\mathcal{R}(\{\mathcal{G}\})$ represents calculating a naive TR in which $\Sigma_i = \mathbf{E}_i$, $i = 1, \dots, d$. Define $\partial \|\mathcal{S}_0\|_1 = \mathcal{E} + \mathcal{N}$, we now show that a small perturbation will increase the value of $f(\mathcal{L}_0, \mathcal{S}_0)$.

$$\begin{aligned} & f(\mathcal{L}_0 + \Delta, \mathcal{S}_0 - \mathcal{P}_\Omega(\Delta)) - f(\mathcal{L}_0, \mathcal{S}_0) \\ & \geq \langle \sum_{i=1}^{\lfloor d/2 \rfloor} w_i \mathcal{A}_{il}^* (\partial \|\mathbf{L}_{\{i,l\}}^{(i)}\|_*), \Delta \rangle - \langle \lambda \partial \|\mathcal{S}_0\|_1, \mathcal{P}_\Omega(\Delta) \rangle \\ & = \langle \mathcal{R} + \sum_{i=1}^{\lfloor d/2 \rfloor} w_i \mathcal{A}_{kl}^* (\mathbf{W}_{\{i,l\}}), \Delta \rangle - \langle \lambda \partial \|\mathcal{S}_0\|_1, \Delta \rangle \\ & = w_k \|\mathcal{P}_{T_{kl}^\perp} (\Delta_{\{k,l\}})\|_* + \lambda_k \|\mathcal{P}_\Psi(\Delta)\|_1 + \\ & \quad \langle \mathcal{Y} + \mathcal{R} - \lambda_k \mathcal{N}, \Delta \rangle - \langle \mathcal{Y}, \Delta \rangle \\ & = w_k \|\mathcal{P}_{T_{kl}^\perp} (\Delta_{\{k,l\}})\|_* + \lambda_k \|\mathcal{P}_\Psi(\Delta)\|_1 + \\ & \quad \langle \mathcal{P}_{T_{kl}} (\mathbf{Y}_{\{k,l\}} + \mathbf{R}_{\{k,l\}} - \lambda_k \mathbf{N}_{\{k,l\}}), \mathcal{P}_{T_{kl}} (\Delta_{\{k,l\}}) \rangle + \\ & \quad \langle \mathcal{P}_{T_{kl}^\perp} (\mathbf{Y}_{\{k,l\}} - \lambda_k \mathbf{N}_{\{k,l\}}), \mathcal{P}_{T_{kl}^\perp} (\Delta_{\{k,l\}}) \rangle - \langle \mathcal{Y}, \mathcal{P}_\Psi(\Delta) \rangle \\ & \geq \frac{w_k}{2} \|\mathcal{P}_{T_{kl}^\perp} (\Delta_{\{k,l\}})\|_* + \frac{\lambda_k}{2} \|\mathcal{P}_\Psi(\Delta)\|_1 - \\ & \quad \prod_{i=1}^d n_i^{-1} \|\mathcal{P}_{T_{kl}} (\Delta_{\{k,l\}})\|_F \end{aligned}$$

The first inequality is attributed to the convexity of nuclear norm and ℓ_1 norm using Taylor expansion. The second equality is due to $\mathcal{P}_{\Omega^\perp}(\partial \|\mathcal{S}_0\|_1) = 0$. Since $\mathcal{P}_{T_{kl}}(\mathbf{W}_{\{k,l\}}) = 0$ and $\mathcal{P}_{\Psi^\perp}(\mathcal{E}) = 0$, let $\mathbf{W}_{\{i,l\}} = \mathbf{0}$, $i \neq k$ and picking up $\mathbf{W}_{\{k,l\}}$ and \mathcal{E} such that $\langle \mathbf{T}_{kl}(\mathbf{W}_{\{k,l\}}), \Delta \rangle = \|\mathcal{P}_{T_{kl}^\perp}(\Delta_{\{k,l\}})\|_*$ and $\langle -\lambda \mathcal{E}, \Delta \rangle = \lambda_k \|\mathcal{P}_\Psi(\Delta)\|_1$ the third equality holds. Expanding the inner product and note that $\mathcal{P}_{T_{kl}^\perp}(\mathbf{R}_{\{k,l\}}) = \mathbf{0}$ the fourth equality holds. The last inequality is because of (21)



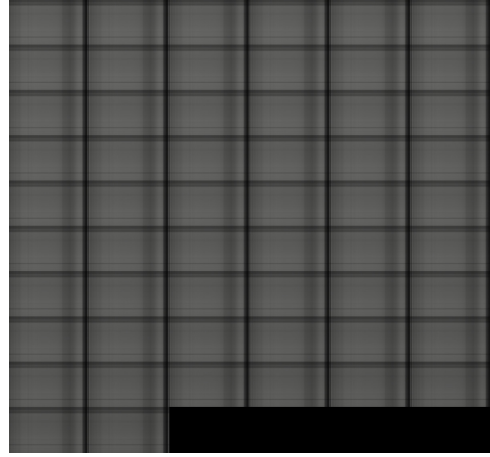
(c) Original video.



(d) Result derived by TRRPCA, and the average recovery time is 135.19s.



(e) Result derived by TRPCA-TNN, and the average recovery time is 208.74s.



(f) Result derived by TRPCA-SNN, and the average recovery time is 220.85s.

 Fig. 2. The recovery result of background separation for *visiontraffic* video yielded by three methods.

and

$$\left\{ \begin{array}{l} \langle \mathcal{P}_{T_{kl}^\perp} (\mathbf{Y}_{\{k,l\}} - \lambda_k \mathbf{N}_{\{k,l\}}), \mathcal{P}_{T_{kl}^\perp} (\Delta_{\{k,l\}}) \rangle \geq \\ - \frac{w_k}{2} \|\mathcal{P}_{T_{kl}^\perp} (\Delta_{\{k,l\}})\|_* \\ \langle \mathcal{P}_{T_{kl}} (\mathbf{Y}_{\{k,l\}} + \mathbf{R}_{\{k,l\}} - \lambda_k \mathbf{N}_{\{k,l\}}), \mathcal{P}_{T_{kl}} (\Delta_{\{k,l\}}) \rangle \geq \\ - \prod_{i=1}^d n_i^{-1} \|\mathcal{P}_{T_{kl}} (\Delta_{\{k,l\}})\|_{\text{F}} \\ \langle \mathcal{Y}, \mathcal{P}_{\Psi} (\Delta) \rangle \geq - \frac{\lambda_k}{2} \|\mathcal{P}_{\Psi} (\Delta)\|_1 \end{array} \right.$$

Since (20) indicates $\|\frac{1}{\sqrt{(1-2\gamma)p}} \mathcal{P}_{T_{kl}} \mathcal{P}_{\Psi_{\{k,l\}}}\|_2 < \sqrt{3/2}$, thus

$$\begin{aligned} & \|\mathcal{P}_{T_{kl}} (\Delta_{\{k,l\}})\|_{\text{F}} \\ & \leq 2 \left\| \frac{1}{(1-2\gamma)p} \mathcal{P}_{T_{kl}} \mathcal{P}_{\Psi_{kl}} \mathcal{P}_{T_{kl}} (\Delta_{\{k,l\}}) \right\|_{\text{F}} \\ & \leq 2 \left\| \frac{1}{(1-2\gamma)p} \mathcal{P}_{T_{kl}} \mathcal{P}_{\Psi_{kl}} \mathcal{P}_{T_{kl}^\perp} (\Delta_{\{k,l\}}) \right\|_{\text{F}} + \\ & \quad 2 \left\| \frac{1}{(1-2\gamma)p} \mathcal{P}_{T_{kl}} \mathcal{P}_{\Psi_{kl}} (\Delta_{\{k,l\}}) \right\|_{\text{F}} \\ & \leq \sqrt{\frac{6}{(1-2\gamma)p}} \|\mathcal{P}_{T_{kl}^\perp} (\Delta_{\{k,l\}})\|_{\text{F}} + \\ & \quad \sqrt{\frac{6}{(1-2\gamma)p}} \|\mathcal{P}_{\Psi_{kl}} (\Delta_{\{k,l\}})\|_{\text{F}}. \end{aligned}$$

Without loss of generality, assume $\prod_{i=1}^d n_i$ is sufficient large

and we have

$$\begin{aligned} & f(\mathcal{L}_0 + \Delta, \mathcal{S}_0 - \mathcal{P}_\Omega(\Delta)) - f(\mathcal{L}_0, \mathcal{S}_0) \\ & \geq \left(\frac{w_k}{2} - \sqrt{\frac{6}{(1-2\gamma)p}} \prod_{i=1}^d n_i^{-1} \right) \|\mathcal{P}_{T_{kl}^\perp}(\Delta_{\{k,l\}})\|_* + \\ & \quad \left(\frac{\lambda_k}{2} - \sqrt{\frac{6}{(1-2\gamma)p}} \prod_{i=1}^d n_i^{-1} \right) \|\mathcal{P}_\Psi(\Delta)\|_1 \\ & \geq 0. \end{aligned}$$

Since the $\mathcal{P}_{\Psi_{kl}} \mathcal{P}_{T_{kl}}$ satisfies injective property when p and γ are small such that $\|\mathcal{P}_{\Psi_{kl}} \mathcal{P}_{T_{kl}}\|_2 \leq \sqrt{3(1-2\gamma)p/2} < 1$, the equality holds if and only if $\Delta = \mathcal{O}$.

The next step is to construct the dual certificate via the Golf scheme introduced in [1]. To show this, we prove the following conditions.

$$\left\{ \begin{array}{l} \|\mathcal{P}_{T_{kl}}(\mathbf{Y}_{\{k,l\}}) - \mathcal{P}_{T_{kl}}(\lambda_k \mathbf{N}_{\{k,l\}} - \mathbf{R}_{\{k,l\}})\|_F \leq \frac{1}{2} \prod_{i=1}^d n_i^{-1} \\ \|\mathcal{P}_{T_{kl}^\perp}(\mathbf{Y}_{\{k,l\}})\|_2 \leq \frac{w_k}{8\lambda_k} \\ \|\mathcal{P}_{T_{kl}^\perp}(\mathbf{E}_{\{k,l\}})\|_2 \leq \frac{w_k}{8\lambda_k} \\ \|\mathbf{Y}_{\{k,l\}}\|_\infty \leq \frac{\lambda_k}{2} \end{array} \right. \text{by taking } t = O\left(\sqrt{p\mu r_k r_{k+l} \ln(\bar{n}_{kl})/\underline{n}_{kl}}\right), \text{ which implies} \quad (22)$$

Since $\Psi = \bigcup_{i=1}^{j_0} \Psi^i$ can be regarded as a union of several support sets that obey the Bernoulli distribution $\Psi^i \sim \text{Ber}(q_i)$. Specifically define $q_1 = q_2 = (1-2\gamma)p/6$ and $q_3 = \dots = q_{j_0} = q$ where $q > C_r p / \ln(\bar{n}_{kl})$. Consider the probability of one entry being chosen there is $1 - (1-2\gamma)p = ((1-2\gamma)p/6)^2 (1-q)^{j_0-2}$, $j_0 = \lceil 5 \ln(n) + 1 \rceil$. Inductively define

$$\mathcal{Y}^j = \begin{cases} \mathbf{Z}_{\{k,l\}}^0 = \mathcal{P}_{T_{kl}}(\lambda_k \mathbf{E}_{\{k,l\}} - \mathbf{R}_{\{k,l\}}) \\ \mathcal{Y}^j = \sum_{i=1}^j q_i^{-1} \mathcal{P}_{\Psi^i}(\mathcal{Z}^{j-1}) \\ \mathbf{Z}_{\{k,l\}}^j = \mathbf{Z}_{\{k,l\}}^0 - \mathcal{P}_{T_{kl}}(\mathbf{Y}_{\{k,l\}}^j) \end{cases},$$

where the third term can be rewritten as $\mathbf{Z}_{\{k,l\}}^j = (\mathcal{P}_{T_{kl}} - q_j^{-1} \mathcal{P}_{T_{kl}} \mathcal{P}_{\Psi^j} \mathcal{P}_{T_{kl}})(\mathbf{Z}_{\{k,l\}}^{j-1})$. Accordingly the following conditions satisfied:

$$\left\{ \begin{array}{l} \|\mathcal{Z}^j\|_F \leq 2^{-1} \|\mathcal{Z}^{j-1}\|_F, \\ \|\mathcal{Z}^1\|_\infty \leq 2^{-1} \ln^{-1/2}(\bar{n}_{kl}) \|\mathcal{Z}^0\|_\infty, \\ \|\mathcal{Z}^j\|_\infty \leq 2^{-j} \ln^{-1}(\bar{n}_{kl}) \|\mathcal{Z}^{j-1}\|_\infty, \\ \|(\mathcal{E} - q_j^{-1} \mathcal{P}_{\Psi^j})(\mathcal{Z}^{j-1})\|_2 \leq C \sqrt{\bar{n}_{kl} \ln(\bar{n}_{kl})} / q_j \|\mathcal{Z}^{j-1}\|_\infty \end{array} \right.$$

To bound $\|\mathcal{Z}^0\|_F$ and $\|\mathcal{Z}^0\|_\infty$, we first resort to $\|\mathcal{Z}^0\|_\infty \leq \|\mathcal{P}_{T_{kl}}(\mathbf{E}_{\{k,l\}})\|_\infty + \|\mathbf{R}_{\{k,l\}}\|_\infty$. Recall that $\|\mathcal{P}_{T_{kl}}(\mathbf{I}_{\{k,l\},mn})\|_\infty \leq 2\mu r_k r_{k+l} / \underline{n}_{kl}$ and $\|\mathcal{P}_{T_{kl}}(\mathbf{I}_{\{k,l\},mn})\|_F \leq \sqrt{2\mu r_k r_{k+l} / \underline{n}_{kl}}$, in which $\mathbf{I}_{\{k,l\},mn} = \mathbf{e}_{\{k,l\},m} \mathbf{e}_{\{k+l,d-l\},n}^\top$ and μ is defined in

[22]. Using the Bernstein's inequality, we deduce

$$\begin{aligned} & \Pr(|\langle \mathcal{P}_{T_{kl}}(\mathbf{E}_{\{k,l\}}), \mathbf{I}_{\{k,l\},mn} \rangle| > t) \\ & = \Pr(|\langle \mathbf{E}_{\{k,l\}}, \mathcal{P}_{T_{kl}}(\mathbf{I}_{\{k,l\},mn}) \rangle| > t) \\ & \leq 2e^{-\frac{t^2/2}{v+Ct/3}}, \end{aligned}$$

since $V = 2\gamma p \|\mathcal{P}_{T_{kl}}(\mathbf{I}_{\{k,l\},mn})\|_F^2 \leq 4\gamma p \mu r_k r_{k+l} / \underline{n}_{kl}$ and $C = \|\mathcal{P}_{T_{kl}}(\mathbf{I}_{\{k,l\},mn})\|_\infty \leq 2\mu r_k r_{k+l} / \underline{n}_{kl}$, then

$$\begin{aligned} & \Pr(|\langle \mathcal{P}_{T_{kl}}(\mathbf{E}_{\{k,l\}}), \mathbf{I}_{\{k,l\},mn} \rangle| > t) \\ & \leq 2e^{-\frac{\sqrt{p} \ln(\bar{n}_{kl})/4}{2\gamma \sqrt{p} + \sqrt{\mu r_k r_{k+l} \ln(\bar{n}_{kl})/\underline{n}_{kl}}}} \\ & < 2e^{-\frac{\sqrt{p} \ln(\bar{n}_{kl})/4}{2\gamma \sqrt{p} + \sqrt{\mu \ln(\bar{n}_{kl})}}} \\ & < 2e^{-\sqrt{p} \ln(\bar{n}_{kl})/\mu/8} \\ & < 2e^{-\sqrt{p(\mu'')^{-1} \ln(\bar{n}_{kl})}/8} \\ & = 2e^{-C \ln^{1/4}(\bar{n}_{kl})} \end{aligned}$$

$\|\mathcal{P}_{T_{kl}}(\mathbf{E}_{\{k,l\}})\|_\infty \leq C_1 \sqrt{p\mu r_k r_{k+l} \ln(\bar{n}_{kl})/\underline{n}_{kl}}$. Note that $\|\mathbf{R}_{\{k,l\}}\|_\infty = \|\mathcal{R}\|_\infty \leq \sum_{i=1}^{\lceil d/2 \rceil} w_i r_i r_{i+l} \prod_{i=1}^d \sqrt{\mu_{B_i}/n_i} = C_2 \sqrt{u''/\bar{n}_{kl} \underline{n}_{kl}} \leq C_2 \sqrt{\mu r_k r_{k+l} / \underline{n}_{kl}}$, accordingly we have $\|\mathcal{Z}^0\|_\infty \leq (C_1 + C_2) \sqrt{\mu r_k r_{k+l} \ln(\bar{n}_{kl})/\underline{n}_{kl}}$ and $\|\mathcal{Z}^0\|_F \leq \sqrt{\bar{n}_{kl} \underline{n}_{kl}} \|\mathcal{Z}^0\|_\infty \leq (C_1 + C_2) \sqrt{\mu r_k r_{k+l} \bar{n}_{kl} \ln(\bar{n}_{kl})}$.

The second step is to bound $\|\mathcal{P}_{T_{kl}^\perp}(\mathbf{Y}_{\{k,l\}}^{j_0})\|_2$. We deduce it like follows:

$$\begin{aligned} & \|\mathcal{P}_{T_{kl}^\perp}(\mathbf{Y}_{\{k,l\}}^{j_0})\|_2 \\ & \leq \sum_{i=1}^{j_0} \|q_i^{-1} (\mathcal{P}_{T_{kl}^\perp} \mathcal{P}_{\Psi^i})(\mathbf{Z}_{\{k,l\}}^{i-1})\|_2 \\ & \leq \sum_{i=1}^{j_0} \|q_i^{-1} (\mathcal{P}_{T_{kl}^\perp} - \mathcal{E})(\mathbf{Z}_{\{k,l\}}^{i-1})\|_2 \\ & \leq C \sum_{i=1}^{j_0} \sqrt{q_i^{-1} \bar{n}_{kl} \ln(\bar{n}_{kl})} \|\mathbf{Z}_{\{k,l\}}^{i-1}\|_\infty \\ & \leq C \sqrt{\bar{n}_{kl} \ln(\bar{n}_{kl})} \|\mathbf{Z}_{\{k,l\}}^0\|_\infty \\ & \quad \left(\frac{1}{\sqrt{q_1}} + \frac{2^{-1}}{\sqrt{q_2 \ln(\bar{n}_{kl})}} + \sum_{i=3}^{j_0} \frac{2^{1-i}}{\sqrt{q_i \ln(\bar{n}_{kl})}} \right) \\ & \leq C (C_1 + C_2) \sqrt{p^{-1} \mu r_k r_{k+l} \bar{n}_{kl} \ln^2(\bar{n}_{kl}) \underline{n}_{kl}^{-1}} \\ & \leq C (C_1 + C_2) \sqrt{p^{-1} \mu'' r_k r_{k+l} \bar{n}_{kl} \ln^3(\bar{n}_{kl}) \underline{n}_{kl}^{-1}} \\ & \leq C \sqrt{C_p^{-1} \bar{n}_{kl}} \\ & \leq w_k (8\lambda_k)^{-1}, \end{aligned}$$

provided that $C_p = p \underline{n}_{kl} (\mu'' r_k r_{k+l})^{-1} (C_1 + C_2)^{-2} \ln^{-3}(\bar{n}_{kl})$ is large enough.

The third step is to bound $\|\mathcal{P}_{T_{kl}^\perp}(\mathbf{E}_{\{k,l\}})\|_2$ which is naturally derived from $\|\mathcal{P}_{T_{kl}^\perp}(\mathbf{E}_{\{k,l\}})\|_2 \leq \|\mathbf{E}_{\{k,l\}}\|_2 \leq w_k (8\lambda_k)^{-1}$.

The fourth step is to bound $\|\mathbf{Y}_{\{k,l\}}^{j_0}\|_\infty$. We prove it like

follows:

$$\begin{aligned}
 & \|\mathbf{Y}_{\{k,l\}}^{j_0}\|_\infty \\
 & \leq \sum_{i=1}^{j_0} \|q_i^{-1} (\mathcal{P}_{T_{kl}^\perp} \mathcal{P}_{\Psi^i}) (\mathbf{z}_{\{k,l\}}^{i-1})\|_\infty \\
 & \leq \sum_{i=1}^{j_0} \|q_i^{-1} (\mathcal{P}_{T_{kl}^\perp} - \mathcal{E}) (\mathbf{z}_{\{k,l\}}^{i-1})\|_\infty \\
 & \leq C \sum_{i=1}^{j_0} q_i^{-1} \|\mathbf{z}_{\{k,l\}}^{i-1}\|_\infty \\
 & \leq \left(\frac{1}{\sqrt{q_1}} + \frac{2^{-1}}{\sqrt{q_2 \ln(\bar{n}_{kl})}} + \sum_{i=3}^{j_0} \frac{2^{1-i}}{\sqrt{q_i \ln(\bar{n}_{kl})}} \right) \|\mathbf{z}_{\{k,l\}}^0\|_\infty \\
 & \leq (C_1 + C_2) \sqrt{p^{-1} \mu r_k r_{k+l} \ln(\bar{n}_{kl}) \underline{n}_{kl}^{-1}} \\
 & \leq (C_1 + C_2) \sqrt{p^{-1} \mu'' r_k r_{k+l} \underline{n}_{kl}^{-1} (\ln(\bar{n}_{kl}) + \ln(\underline{n}_{kl}))} \\
 & \leq \sqrt{C_p^{-1} \ln^{-1}(\bar{n}_{kl})} \\
 & \leq 1/4,
 \end{aligned}$$

in which C_p is required to be large enough.

The final step is to prove the first condition in (22). We show it like this:

$$\begin{aligned}
 & \|\mathcal{P}_{T_{kl}} (\mathbf{Y}_{\{k,l\}}^{j_0}) - \mathcal{P}_{T_{kl}} (\lambda_k \mathbf{N}_{\{k,l\}} - \mathbf{R}_{\{k,l\}})\|_F \\
 & = \|\mathcal{P}_{T_{kl}} (\mathbf{Y}_{\{k,l\}}^{j_0}) - \mathbf{Z}_{\{k,l\}}^0\|_F \\
 & = \|\mathbf{Z}_{\{k,l\}}^{j_0}\|_F \\
 & \leq C 2^{-j_0} \|\mathbf{Z}_{\{k,l\}}^0\|_F \\
 & \leq C \bar{n}_{kl}^{-5} \sqrt{\mu r_k r_{k+l} \bar{n}_{kl} \ln(\bar{n}_{kl})} \\
 & \leq \frac{1}{2} \prod_{i=1}^d n_i^{-1}.
 \end{aligned}$$

The proof is complete. \square

APPENDIX B PROOF OF LEMMA 1

Proof. Denote by $\mathbf{A} \in \mathbb{R}^{m \times \prod_{i=1}^d n_i}$ the matrix form of linear mapping \mathcal{A}_Ω , where $\Omega = \{j_1, \dots, j_m\}$ and $\mathbf{A} = [\mathbf{e}_{j_1}, \dots, \mathbf{e}_{j_m}]^\top$, $1 \leq j_i \leq m$, $\forall i \in [m]$. The aforementioned optimization becomes

$$\min_{\mathcal{A}} \frac{1}{2} \|\mathbf{A} \text{Vec}(\mathcal{X}) - \mathbf{A} \text{Vec}(\mathcal{B})\|_2^2 + \tau \|\text{Vec}(\mathcal{X})\|_1,$$

thus its first-order optimality condition is

$$\mathbf{0} \in \mathbf{A}^\top \mathbf{A} [\text{Vec}(\mathcal{X}) - \text{Vec}(\mathcal{B})] + \tau \partial \|\text{Vec}(\mathcal{X})\|_1,$$

which can be reformulated as

$$\mathbf{0} \in \mathbf{A}^\top \mathbf{A} [\text{Vec}(\mathcal{X}) - \text{Vec}(\mathcal{B})] + \tau \partial \|\mathbf{A}^\top \mathbf{A} \text{Vec}(\mathcal{X})\|_1 + \tau \partial \|(\mathbf{E} - \mathbf{A}^\top \mathbf{A}) \text{Vec}(\mathcal{X})\|_1.$$

Define the projection operator $\mathcal{P}_\Omega = \mathcal{A}_\Omega^* \mathcal{A}_\Omega$ and its matrix expression $\mathbf{P} = \mathbf{A}^\top \mathbf{A}$, where \mathcal{A}^* represents the adjoint of \mathcal{A} .

The formula of optimality condition is

$$\begin{aligned}
 \mathbf{0} \in & \mathcal{P}_\Omega (\text{Vec}(\mathcal{X}) - \text{Vec}(\mathcal{B})) + \tau \partial \|\mathcal{P}_\Omega (\text{Vec}(\mathcal{X}))\|_1 + \\
 & \tau \partial \|\mathcal{P}_{\Omega^\perp} (\text{Vec}(\mathcal{X}))\|_1.
 \end{aligned}$$

In order to minimize the ℓ_1 norm, the value of component under projection Ω^\perp should be 0. Note that the projection satisfies $\mathbf{A}^\top \mathbf{A} = \sum_{i=1}^m \mathbf{e}_{j_i} \mathbf{e}_{j_i}^\top = \text{diag}(\dots, j_1, 0, \dots, j_m, 0, \dots) = \text{diag}(\text{Vec}(\mathcal{P}))$. Rewrite the condition as

$$\mathbf{0} \in \mathcal{P} \otimes \mathcal{X} - \mathcal{P} \otimes \mathcal{B} + \tau \partial \|\mathcal{P} \otimes \mathcal{X}\|_1,$$

which is also the optimality condition of

$$\min_{\mathcal{A}} \frac{1}{2} \|\mathcal{P} \otimes \mathcal{X} - \mathcal{P} \otimes \mathcal{B}\|_F^2 + \tau \|\mathcal{P} \otimes \mathcal{X}\|_1.$$

Since $\text{sgn}(0) = 0$, the optimal solution is $\mathcal{X}^* = \text{S}_\tau(\mathcal{P} \otimes \mathcal{B})$. \square

REFERENCES

- [1] E. J. Candès, X. Li, Y. Ma, and J. Wright, "Robust principal component analysis?," *Journal of the ACM (JACM)*, vol. 58, no. 3, p. 11, 2011.
- [2] A. Cichocki, D. Mandic, L. De Lathauwer, G. Zhou, Q. Zhao, C. Caiafa, and H. A. Phan, "Tensor decompositions for signal processing applications: from two-way to multiway component analysis," *IEEE Signal Processing Magazine*, vol. 32, no. 2, pp. 145–163, 2015.
- [3] N. D. Sidiropoulos, L. De Lathauwer, X. Fu, K. Huang, E. E. Papalexakis, and C. Faloutsos, "Tensor decomposition for signal processing and machine learning," *IEEE Transactions on Signal Processing*, vol. 65, no. 13, pp. 3551–3582, 2017.
- [4] M. Signoretto, R. Van de Plas, B. De Moor, and J. A. Suykens, "Tensor versus matrix completion: a comparison with application to spectral data," *IEEE Signal Processing Letters*, vol. 18, no. 7, pp. 403–406, 2011.
- [5] J. Liu, P. Musialski, P. Wonka, and J. Ye, "Tensor completion for estimating missing values in visual data," *IEEE Transactions on Pattern Analysis and Machine Intelligence*, vol. 35, no. 1, pp. 208–220, 2013.
- [6] T. G. Kolda and B. W. Bader, "Tensor decompositions and applications," *SIAM Review*, vol. 51, no. 3, pp. 455–500, 2009.
- [7] A. Cichocki, N. Lee, I. Oseledets, A.-H. Phan, Q. Zhao, D. P. Mandic, et al., "Tensor networks for dimensionality reduction and large-scale optimization: part 1 low-rank tensor decompositions," *Foundations and Trends® in Machine Learning*, vol. 9, no. 4-5, pp. 249–429, 2016.
- [8] S. Gandy, B. Recht, and I. Yamada, "Tensor completion and low-n-rank tensor recovery via convex optimization," *Inverse Problems*, vol. 27, no. 2, p. 025010, 2011.
- [9] C. J. Hillar and L.-H. Lim, "Most tensor problems are NP-hard," *Journal of the ACM*, vol. 60, no. 6, p. 45, 2013.
- [10] D. Goldfarb and Z. Qin, "Robust low-rank tensor recovery: Models and algorithms," *SIAM Journal on Matrix Analysis and Applications*, vol. 35, no. 1, pp. 225–253, 2014.
- [11] B. Romera-Paredes and M. Pontil, "A new convex relaxation for tensor completion," in *Advances in Neural Information Processing Systems*, pp. 2967–2975, 2013.
- [12] C. Mu, B. Huang, J. Wright, and D. Goldfarb, "Square deal: Lower bounds and improved relaxations for tensor recovery," in *International Conference on Machine Learning*, pp. 73–81, 2014.
- [13] B. Huang, C. Mu, D. Goldfarb, and J. Wright, "Provable low-rank tensor recovery," *Optimization-Online*, vol. 4252, no. 2, 2014.
- [14] M. E. Kilmer, K. Braman, N. Hao, and R. C. Hoover, "Third-order tensors as operators on matrices: a theoretical and computational framework with applications in imaging," *SIAM Journal on Matrix Analysis and Applications*, vol. 34, no. 1, pp. 148–172, 2013.
- [15] F. Mémoli and G. Sapiro, "A theoretical and computational framework for isometry invariant recognition of point cloud data," *Foundations of Computational Mathematics*, vol. 5, no. 3, pp. 313–347, 2005.
- [16] C. Lu, J. Feng, W. Liu, Z. Lin, S. Yan, et al., "Tensor robust principal component analysis with a new tensor nuclear norm," *IEEE transactions on pattern analysis and machine intelligence*, 2019.
- [17] Q. Zhao, M. Sugiyama, and A. Cichocki, "Learning efficient tensor representations with ring structure networks," *arXiv preprint arXiv:1705.08286*, 2017.

- [18] K. Ye and L.-H. Lim, “Tensor network ranks,” *arXiv preprint arXiv:1801.02662*, 2018.
- [19] J. A. Bengua, H. N. Phien, H. D. Tuan, and M. N. Do, “Efficient tensor completion for color image and video recovery: low-rank tensor train,” *IEEE Transactions on Image Processing*, vol. 26, no. 5, pp. 2466–2479, 2017.
- [20] W. Wang, V. Aggarwal, and S. Aeron, “Efficient low rank tensor ring completion,” in *Computer Vision (ICCV), 2017 IEEE International Conference on*, IEEE, 2017.
- [21] J. Yu, G. Zhou, Q. Zhao, and K. Xie, “An effective tensor completion method based on multi-linear tensor ring decomposition,” in *Proceedings, APSIPA Annual Summit and Conference*, vol. 2018, pp. 12–15, 2018.
- [22] H. Huang, Y. Liu, and C. Zhu, “Provable model for tensor ring completion,” *arXiv preprint arXiv:1903.03315*, 2019.
- [23] Y. Liu, F. Shang, W. Fan, J. Cheng, and H. Cheng, “Generalized higher order orthogonal iteration for tensor learning and decomposition,” *IEEE Transactions on Neural Networks and Learning Systems*, vol. 27, no. 12, pp. 2551–2563, 2016.
- [24] L. Yang, Z.-H. Huang, and X. Shi, “A fixed point iterative method for low n -rank tensor pursuit,” *IEEE Transactions on Signal Processing*, vol. 61, no. 11, pp. 2952–2962, 2013.
- [25] R. Nishihara, L. Lessard, B. Recht, A. Packard, and M. I. Jordan, “A general analysis of the convergence of admm,” *arXiv preprint arXiv:1502.02009*, 2015.
- [26] Z. Lin, M. Chen, and Y. Ma, “The augmented lagrange multiplier method for exact recovery of corrupted low-rank matrices,” *arXiv preprint arXiv:1009.5055*, 2010.
- [27] C. Lu, *A Library of ADMM for Sparse and Low-rank Optimization*. National University of Singapore, June 2016. <https://github.com/canyilu/LibADMM>.
- [28] M. F. Barnsley and L. P. Hurd, *Fractal image compression*, vol. 1. AK peters Wellesley, 1993.
- [29] Z. Wang, E. Simoncelli, A. Bovik, *et al.*, “Multi-scale structural similarity for image quality assessment,” in *ASILOMAR Conference on Signals Systems and Computers*, vol. 2, pp. 1398–1402, IEEE; 1998, 2003.
- [30] J. I. Latorre, “Image compression and entanglement,” *arXiv preprint quant-ph/0510031*, 2005.